

Review

Characteristics and Recent Development of Fluoride Magneto-Optical Crystals

Zhonghan Zhang ¹, Zhen Wu ^{1,2}, Zhen Zhang ¹, Liangbi Su ^{1,2}, Anhua Wu ^{1,2,*}, Yang Li ³ and Jianghe Lan ³

¹ State Key Laboratory of High Performance Ceramics and Superfine Microstructure, Shanghai Institute of Ceramics, Chinese Academy of Sciences, Shanghai 201899, China

² Ganjiang Innovation Academy, Chinese Academy of Sciences, Ganzhou 341000, China

³ Southwest Institute of Applied Magnetism, Mianyang 621010, China

* Correspondence: wuanhua@mail.sic.ac.cn

Abstract: Magneto-optical materials are the fundamental component of Faraday isolators; therefore, they are significantly important for solid-state laser systems. Fluoride magneto-optical crystals such as CeF₃, KTb₃F₁₀ and LiTbF₄ exhibit advantages of wide transmittance range, high optical homogeneity, smaller thermal lensing and weaker thermal induced depolarization effect, and thus are promising candidates for Faraday isolators in high-power solid-state lasers. Recent progress in crystal growth and characterizations of these fluoride magneto-optical crystals are introduced. Possible applications of Faraday isolators based on various fluoride crystals are discussed, especially for solid-state lasers in the ultraviolet (UV) or infrared (IR) spectral region.

Keywords: magneto-optical crystal; fluoride crystal; crystal growth; Faraday isolator

1. Introduction

Magneto-optical materials are the key component of Faraday isolators (FIs), which is of great importance in high-power solid-state laser systems and optical communication techniques [1]. The magneto-optical materials used in the FI devices are often called Faraday rotators. A brief structure of the Faraday isolator is shown in Figure 1. Taking advantage of the Faraday effect of magneto-optical materials, the polarization of the induced polarized light beam will be rotated by the angle

$$\theta = V \cdot B \cdot L \quad (1)$$

where V is the Verdet constant of the magneto-optical material, B is the magnetic flux density along the propagating direction and L is the length of the beam path inside the magneto-optical materials. If the length of magneto-optical materials and the magnetic flux density are designed to produce a rotation angle of $\theta = \pi/4$ (or 45°), the reflected light will be perpendicular to the input polarizer because the polarization of the reflected light beam will be rotated twice when propagating backwards along the magneto-optical materials; thus, the reflect light beam will be completely prevented.

As the light beams can only be propagated along one direction, the FI devices are also known as optical diodes for an optical system. In optical communication techniques, IF devices can prevent backwards-propagated light beams and improve the noise-to-signal ratios [1,2]. Meanwhile, for high-power laser systems, FIs are crucially important for protecting pumping LD sources from being damaged by the scattering laser beams. Furthermore, the beam propagation between adjacent amplifier stages in high-power systems will be completely irreversible when separated by FI devices; therefore, the laser operation within each stage can be more stable by eliminating amplified spontaneous emission (ASE), reducing parasitic oscillations, etc. [3–5].



Citation: Zhang, Z.; Wu, Z.; Zhang, Z.; Su, L.; Wu, A.; Li, Y.; Lan, J. Characteristics and Recent Development of Fluoride Magneto-Optical Crystals. *Magnetochemistry* **2023**, *9*, 41. <https://doi.org/10.3390/magnetochemistry9020041>

Academic Editor: Andrea Cornia

Received: 10 November 2022

Revised: 16 January 2023

Accepted: 21 January 2023

Published: 27 January 2023



Copyright: © 2023 by the authors. Licensee MDPI, Basel, Switzerland. This article is an open access article distributed under the terms and conditions of the Creative Commons Attribution (CC BY) license (<https://creativecommons.org/licenses/by/4.0/>).

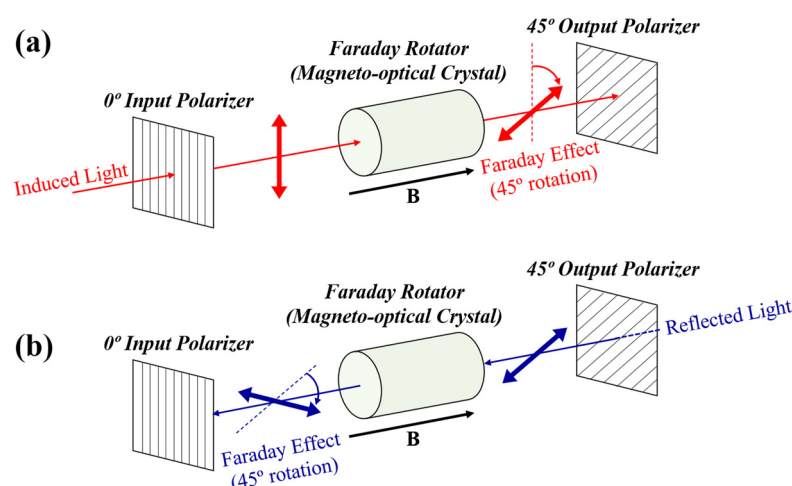


Figure 1. Principle of Faraday isolator using magneto-optical crystals as Faraday rotator. As the polarization of light is rotated by an angle of $\theta = \pi/4$ after propagated through the Faraday rotator, the induced light can pass through the output polarizer (a), meanwhile the reflected light will be shielded by the input polarizer (b).

The main challenge for the power scaling of FI devices in high-power laser systems is thermal effect, e.g., thermal-induced depolarization [6] and the thermal lensing effect [7]. Thus, high thermal conductivity is often considered one of the basic requirements for magneto-optical materials, which is necessary to improve heat dissipation efficiency. Another important requirement of magneto-optical materials is lower propagation losses in order to reduce the distortion of propagated light beams due to local optical absorption. Simultaneously, as the magnitude of thermal effect is proportional to the length of sample, a larger Verdet constant of magneto-optical materials is thus favorable as a smaller L is allowed according to Formula (1).

Considering both the requirements for intrinsic properties and the difficulty of manufacturing high-quality crystals, magneto-optical materials such as terbium gallium garnet ($\text{Tb}_3\text{Ga}_5\text{O}_{12}$, GGG) and yttrium iron garnet ($\text{Y}_3\text{Fe}_5\text{O}_{12}$, YIG) crystals were widely used for FI devices within the visible-to-near-infrared (NIR) spectral range and mid-infrared (mid-IR) spectral range, respectively [8,9]. Faraday rotators using TGG crystals have been widely used in high-power laser systems based on $\text{Nd}^{3+}/\text{Yb}^{3+}$ -doped laser materials or Ti:sapphire crystals. High-quality TGG crystal samples of apertures as large as $\Phi 40$ mm have been reported [10]. However, the development of TGG-based FI devices of a larger aperture is often limited by the dimension of available TGG crystals as well as the thermal effect of larger Faraday rotators, which is considered a potential bottleneck of high-power laser techniques. In addition, the absorption bands of Tb^{3+} within the UV range below 390 nm, in the visible range around 488 nm (${}^7\text{F}_6 \rightarrow {}^5\text{D}_4$), as well as in the IR range over 2.1 μm also limit its applicant spectral range [11].

YIG-based FI devices, on the other hand, exhibit excellent compactness, taking advantage of its high Verdet constant, therefore are often used to fabricate compact and integrated isolators for optical fibers [12]. The excellent transmittance of YIG crystals within the IR spectral range from 1.1 μm until 5 μm also allows its application in the mid-IR spectral range [13]. The main obstacle to producing large-aperture YIG FI devices is the difficulty of growing large-scale YIG crystals due to its incongruent melting characteristics. Although various crystal growth techniques, including the flux method [14], float-zone method [15] as well as the liquid phase epitaxial method [16], have been developed to fabricate YIG crystals or films, the growth of large-volume YIG crystals is still a bottleneck for the development of high-power systems, especially for application in a high-power mid-IR laser facility.

Under this circumstance, efforts to develop novel magneto-optical materials are frequently proposed, which can be divided into two categories. One is mainly aimed for the

application of laser systems of higher average or peak power within the visible to NIR range by solving the limitation of FI device aperture or reducing the thermal effect [17]. Several fluoride crystals, such as $\text{KTb}_3\text{F}_{10}$ [18], TbF_3 [19] and LiTbF_4 [20], exhibit high Verdet constants and low propagation losses, thus are frequently investigated recently. It is worth noticing that these fluoride crystals have small/negative thermo-optic coefficients, which are favorable to inhibit thermal effects by reducing the inhomogeneity of thermal dissipation and compensate for thermal-induced distortion [21]. The other category is to develop novel magneto-optical crystals for potential applications in UV or mid-IR laser systems. Indeed, several fluoride crystals, such as PrF_3 [11] and EuF_2 [22] have wide transmittance ranges and high Verdet constants [6,7,23,24] and therefore constitute an important category of magneto-optical materials for high-power laser systems. In the following paragraphs, the development and state of the art of these fluoride magneto-optical crystals will be introduced. The applications and prospects of several fluoride magneto-optical crystals will be introduced briefly.

2. Terbium (Tb^{3+})-Containing Fluoride Magneto-Optical Crystals for High-Power Laser Applications

2.1. $\text{KTb}_3\text{F}_{10}$ (KTF) and LiTbF_4 (TLF) Crystal

Many magneto-optical materials are paramagnetic compounds containing rare earth (RE) ions, and the magnetic susceptibility of the RE nucleus in the materials is strongly related to its Verdet constant. Terbium-containing fluoride crystals have thus been frequently investigated recently as Tb^{3+} often shows higher susceptibility over other trivalent RE ions [25]. Among the terbium containing fluorides, ternary compounds $\text{KTb}_3\text{F}_{10}$ (KTF) and LiTbF_4 (TLF) are most attractive [26]. Although the potential of KTF and TLF crystals for Faraday rotators had already been reported in the 1970s, e.g., Griffin et al. [27] and Weber et al. [28] reported the magneto-optical properties of both crystals in 1978, substantial development of these crystals for large-aperture FI devices has occurred after the first decades of this century. In 2012, Vasyliov et al. [20] reported a series of fluoride magneto-optical crystals, LiREF_4 (RE = Tb, Dy, Ho, Er and Yb). In 2016, Stevens et al. [26] from Northrop Grumman SYNOPTICS reported the optical and magneto-optical properties of both KTF and TLF crystals, pointing out that “KTF has reduced depolarization for higher laser powers and a smaller focal shift than TGG” [26] under similar experimental conditions, indicating it is a promising candidate for high-power laser applications.

TLF belongs to the tetragonal scheelite structure of space group $I4_1/a$, consistent with the widely used laser host lattice LiYF_4 (YLF). The crystal growth behavior of TLF is also similar to that of YLF due to its similar incongruent melting characteristics [29]. The Czochralski method is the most widely used crystal growth technique for TLF; meanwhile, the excess of LiF in the starting materials could be as high as 63% [30], much higher than the typical growth condition of YLF [31], mainly due to larger deviation of TLF composition away from the eutectic point of the LiF- TbF_3 system. Nevertheless, a large-aperture TLF crystal boule of Φ 40 mm with a length of 70 mm can be fabricated using the conventional crystal growth technique.

KTF belongs to the cubic structure of space group $Fm\bar{3}m$, the same as the laser host KY_3F_{10} (KYF). However, the melting characteristic of KTF is incongruent, differing from KYF [32,33]. The original attempts at KTF crystal growth mainly employed the Czochralski method using a mixture of 30 mol% KF and 70 mol% TbF_3 as starting materials [28]. Top-seeded solution growth (TSSG) [26] and vertical Bridgman (VB) techniques [33] have been used recently to grow KTF crystals. A large-aperture TLF crystal boule of Φ 30 mm with a length of 40 mm was reported by Northrop Grumman SYNOPTICS in 2016 [26].

As the applications of TLF and KTF crystals, i.e., large-aperture FI devices for high-power lasers in the NIR region, are quite similar to those of TGG crystals, the Verdet constants of those crystals are compared with those of TGG in Figure 2. The Verdet constants and optical and thermal properties of these crystals are listed in Table 1. The Verdet constants of these Tb^{3+} -containing ternary compounds at 1.06 μm are $\text{TLF} > \text{TGG}$

> KTF; however, the differences are rather small, indicating the design and geometry of FI devices based on these crystals can be very similar. Recent investigations indicated the extinction value of KTF-based FI devices can reach 30~40 dB at low input power and remains above 20 dB when propagated by a laser beam of power over 370 W [18,26], better than TGG-based devices under the same experimental condition. Despite the fact that the thermal conductivities of these fluoride crystals are obviously lower than those of TGG, as shown in Table 1, the excellent performances of KTF-based FI devices mainly benefit from the small and negative thermo-optical coefficient (dn/dT in Table 1), reducing the thermal effects by compensating for thermal lensing.

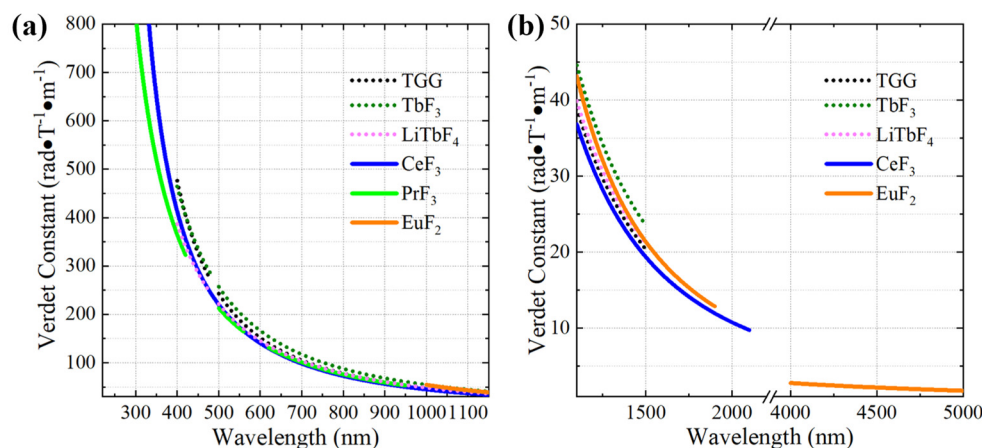


Figure 2. Verdet constants of several fluoride magneto-optical materials in UV-visible-NIR range (a) and mid-IR range (b). The dotted lines correspond with Tb^{3+} -containing materials, whereas the Verdet constant dispersions of other magneto-optical materials are plotted by solid lines. The Verdet constant dispersions are plotted only within the transmittance range.

Table 1. Verdet constant and optical and mechanic properties of fluoride magneto-optical crystals.

	Lattice Type	Thermal Conductivity ($W \cdot m^{-1} \cdot K^{-1}$)	Refractive Index (@ 1.06 μm)	dn/dT ($\times 10^{-6} K^{-1}$ @ 300 K)	Verdet Constant ($Rad \cdot m^{-1} \cdot T^{-1}$)	Transmittance Range
TGG	cubic	4.94 [34,35]	1.94 [18]	17.5 [34]	41.7 @ 1.06 μm 133.2 @ 633 nm 20.39 @ 1.5 μm [11]	
LiTbF ₄	tetragonal	-	$n_o = 1.468$ $n_e = 1.497$ [20]	-5.67 [30]	42.7 @ 1.06 μm [20]	400 nm~1.5 μm (480~500 nm excepted)
KTb ₃ F ₁₀	cubic	1.67 [30]	1.50 [18]	~1 [26]	34 @ 1.06 μm [18]	
TbF ₃	tetragonal	-	$n_x = 1.602$ $n_y = 1.588$ $n_z = 1.569$ (@ 589 nm [36])	-	48 @ 1.06 μm [19]	
CeF ₃	trigonal	2.51// -c [37] 1.92 \perp c [37]	$n_o = 1.6217$ $n_e = 1.6147$ (@ 531 nm [38])	-	39.5 @ 1.06 μm [11]	300 nm~2.1 μm
PrF ₃	trigonal	-	$n_o = 1.6240$ $n_e = 1.6179$ (@ 531 nm [38])	-	125.3 @ 633 nm [11]	220~420 nm 500~560 nm 620~950 nm
EuF ₂	cubic	2.13 [39]	1.555 [40]	-	21.36 @ 1.5 μm [22]	1~7 μm (Eu ³⁺ absorption excepted) [22]

2.2. Other Tb^{3+} -Containing Fluoride Magneto-Optical Crystals

As the Faraday effect of paramagnetic Tb^{3+} -containing crystals is mainly contributed by Tb^{3+} , increasing the density of rare earth sites is a reasonable strategy for improving the Verdet constant. TbF_3 crystals, whose Tb^{3+} densities ($N_{Tb} = 2 \times 10^{22} \text{ cm}^{-3}$) are obviously higher than TGG ($N_{Tb} = 1.275 \times 10^{22} \text{ cm}^{-3}$), TYF ($N_{Tb} = 1.365 \times 10^{22} \text{ cm}^{-3}$) and KYF ($N_{Tb} = 1.487 \times 10^{22} \text{ cm}^{-3}$) crystals, are expected to have higher Verdet constants. In 2017, Valiev et al. reported the synthesis of TbF_3 crystals by vertical Bridgman method [36]. As indicated in Figure 2 and Table 1, the Verdet constant of TbF_3 is higher than that of TGG [19]. However, the attempts of using TbF_3 crystals for FI devices are dramatically limited by its low symmetry. Indeed, TbF_3 is a biaxial crystal with a monoclinic space group $Pnma$. As the propagation direction of Faraday rotators should be parallel with the optical axes for non-cubic materials in order to avoid the influence of birefringence, fabricating a TbF_3 crystal for FI devices is quite difficult because its optical axes differ from all the crystallographic axes.

$Na_{0.37}Tb_{0.63}F_{2.26}$ (NTF) is another novel Tb^{3+} -containing fluoride magneto-optical crystal of high Tb^{3+} density ($N_{Tb} = 1.456 \times 10^{22} \text{ cm}^{-3}$) and belongs to a cubic $Fm\bar{3}m$ space group. Karimov et al. reported the crystal growth of NTF by the Bridgman method in 2014 [41] and afterwards investigated its thermo-optical characteristics in 2015 [42]. The thermo-optical constant dn/dT was found to be very small ($3.44 \times 10^{-6} \text{ K}^{-1}$). After analyzing the performance of IF devices based on NTF crystals of various orientations, it is indicated that NIF based FI devices with isolation ratios larger than 30 dB for propagation power kilowatts level were possible to be obtained [43].

3. Novel Fluoride Magneto-Optical Crystals for UV or MIR Laser Applications

3.1. CeF_3 —Faraday Rotators for High-Power System from UV to MIR Spectral Range

CeF_3 is a uniaxial crystal of a trigonal space group of $P\bar{3}c1$. CeF_3 had exhibited excellent radiation hardness and thus is considered as a potential scintillator for calorimeters [44,45]. Scintillation cylinders which are 30 cm long have been synthesized for potential application in high-energy physics facilities [46], indicating, on the other hand, that it is technically feasible to grow large-size CeF_3 by conventional crystal growth techniques such as the Czochralski process and the vertical Bridgman method.

As shown in Figure 2 and Table 1, the Verdet constant of CeF_3 is slightly lower but very close to that of TGG at $1.06 \mu\text{m}$ [11,47]. In the $\sim 1 \mu\text{m}$ spectral region, the CeF_3 -based FI devices exhibit excellent performances, benefiting from its thermo-optical characteristics even though the thermal conduction of CeF_3 is obviously lower than TGG [6,7]. In 2019, Starobor et al. reported a CeF_3 -based FI device of over 30 dB isolation degree at an average laser power of 700 W, indicating CeF_3 is also a promising Faraday rotator for high-power laser systems even in the NIR region [24].

Additionally, as shown in Figure 3a, CeF_3 exhibits high transmittance continuously from 300 nm to over $2.5 \mu\text{m}$, thus is a promising Faraday rotator material in both the UV region [20] and mid-IR range [48,49]. Indeed, considering the fast development of a 355 nm solid-state UV laser [50,51] and the urgent demand for high-power MIR laser sources in the near future [52], large-aperture FI devices based on CeF_3 crystals could be of crucial importance in both the UV and mid-IR spectral regions.

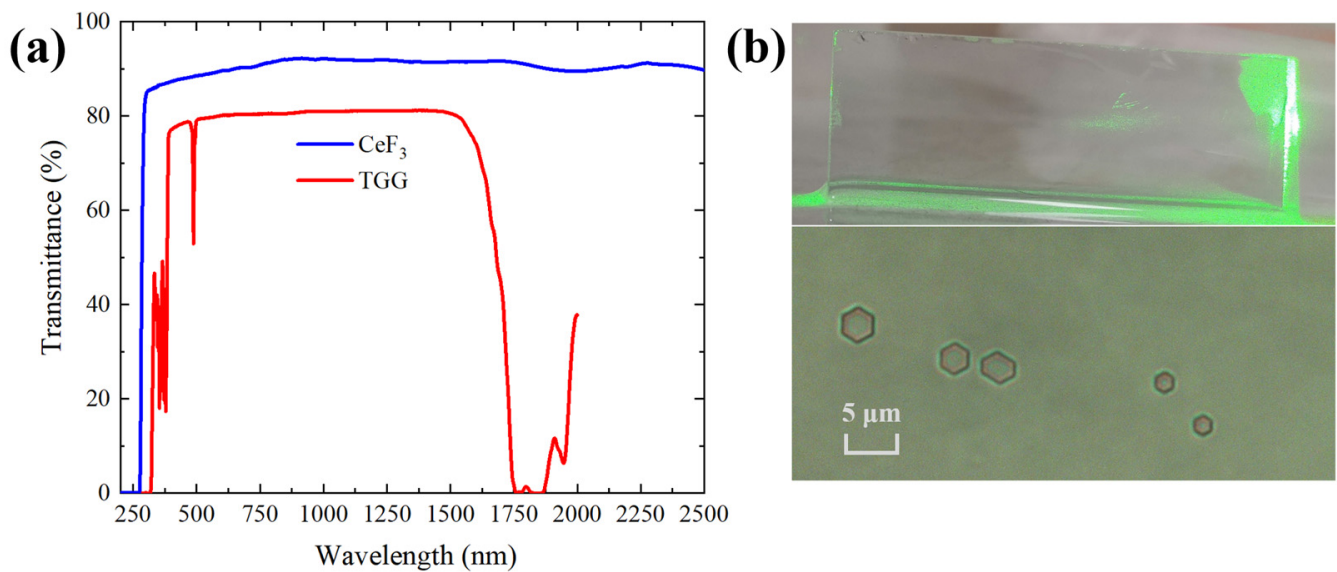


Figure 3. The transmittance spectra of CeF_3 crystal compared with that of TGG crystal (a) [49], and the scattering defects in CeF_3 crystal observed by green laser beam as well as optical microscope (b).

3.2. Absorption-Related Defects in CeF_3

The absorption caused by localized defects will lead to the inhomogeneity of temperature distribution, and therefore is an important origin of thermal effects for magneto-optical crystals. Thus, it is important to reduce these absorption-related defects in magneto-optical crystals. Similar to other fluoride crystals, the contamination of oxygen impurity during the crystal growth of CeF_3 will have an obvious influence on its transmittance [49]. The strict control of oxygen contamination during crystal growth at a high-temperature stage is necessary to obtain CeF_3 crystals with high transmittance.

Scattering centers are another category of defects that will cause local absorption. The influence of these defects can be observed macroscopically by the scattering of laser beams propagated through the CeF_3 crystals, as shown in Figure 3b. Meanwhile, hexagonal hallow structures of millimeter size can be observed inside the crystal by an optical microscope. The shape and symmetry of these defects are consistent with the crystal structure of CeF_3 . The scattering due to these hallow structure defects will give rise to serious local attenuation; thus, it is very important to improve the purity of crystal growth atmosphere and decrease the pulling rate of the crucible in the vertical Bridgman crystal growth process in order to inhibit the formation of these defects.

Using optimized crystal growth parameters, large-size CeF_3 crystals of high quality were grown by Shanghai Institute of Ceramics, Chinese Academy of Sciences. As shown in the inset of Figure 4, crystallographic $-c$ axis cut CeF_3 crystals with apertures larger than 20 mm have been obtained. The performance of the FI device using the $\Phi 15$ mm CeF_3 sample was investigated, as shown in Figure 4. The Faraday rotation angle increases linearly with magnetic field strength.

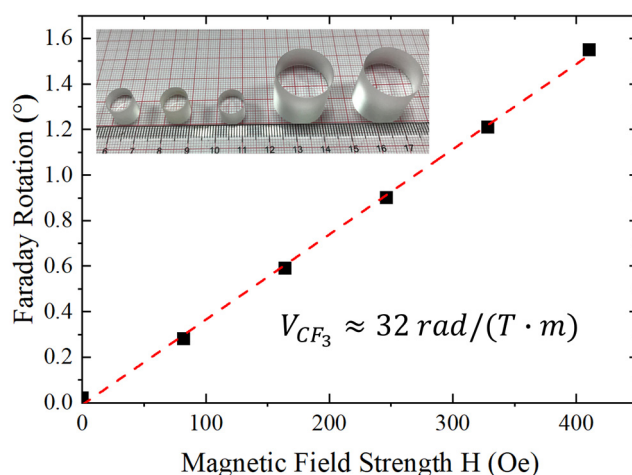


Figure 4. The Faraday rotation angle dependence on the magnetic field strength of CeF_3 Faraday rotators.

3.3. PrF_3 —Potential Faraday Rotators for UV Applications

Similar to CeF_3 , PrF_3 is a uniaxial crystal of a LaF_3 -type trigonal space group of $P\bar{3}c1$ [53]. Molina et al. reported the crystal growth and magneto-optical properties of PrF_3 in 2011 [11]. Although magneto-optical crystals such as LiYbF_4 exhibit UV cut-off even at shorter wavelengths, the PrF_3 crystal is still considered as the best candidate for Faraday rotators from 220 nm to over 300 nm, combining both high transmittance and large Verdet constants, as shown in Figure 2 and Table 1. The appearance of a PrF_3 crystal is green-colored due to the absorption bands from the ground state to the $^3P_{0,1,2}/^1I_6$ states (420 nm~500 nm) and the 1D_2 state (560 nm~620 nm) in the visible region [54]. Under this circumstance, the applicable spectral range of PrF_3 -based Faraday rotators is strictly limited to avoid those absorption peaks. Nevertheless, as reported in Reference [11], PrF_3 is the only candidate for FI devices in the UV region below 300 nm.

3.4. EuF_2 -based Magneto-Optical Materials for MIR Lasers

The magneto-optical properties of $\text{EuF}_{2.11}$, one typical composition of an EuF_2 -based compound, were reported firstly in 2019 by Mironov et al. [22]. The Verdet constant of $\text{EuF}_{2.11}$ crystal is $12.3 \text{ rad} \cdot \text{m}^{-1} \cdot \text{T}^{-1}$ at $2 \mu\text{m}$, which is sufficient for the fabrication of FI devices. Moreover, the wide transmittance of $1\sim 7 \mu\text{m}$ indicates the potential application of EuF_2 in the mid-IR or even long-wave IR range. The most crucial obstacle to be solved associated with this material is the synthesis of a high-purity EuF_2 compound. Indeed, Eu^{3+} is the most stable valence state for europium in fluoride compounds and can be hardly removed completely in the reduction chemical reaction process. The residual Eu^{3+} will generate a series of absorption bands within the $2\sim 4 \mu\text{m}$ range and significantly influence the application of EuF_2 -based magneto-optical materials in this region.

4. Discussion

4.1. The Analysis of Thermal Effect in Fluoride Magneto-Optical Crystals

The interactions between laser beams and magneto-optical crystals of FI devices are transient phenomena rather than absorption/emission processes in the laser gain materials; thus, the most influential thermal effect is thermal lensing and thermally induced depolarization. As these thermal effects are mainly due to the inhomogeneity of temperature distribution that is caused by the local absorption of the propagated laser beam, it is possible to inhibit them by employing magneto-optical crystals of higher thermal conductivity, as was by decreasing those defects that introduce local absorption, as discussed for CeF_3 crystals in Section 3.2. Nevertheless, some other characteristics, such as optical anisotropy and the thermo-optical coefficient, also have crucial influence on the performances of FI devices.

For the thermal lensing effect, the focal length of the thermal lens F can be defined as [6]:

$$\frac{1}{F} = \frac{1}{4\pi a^2} \frac{\alpha L}{\kappa} P \cdot P_0 \quad (2)$$

where a is the beam radius, α is the absorption coefficient, κ is the thermal conductivity and P_0 is the induced laser power. In Formula (2), P is a thermo-optical-related constant, which can be defined for the isotropic materials as [7]:

$$P = \frac{dn}{dT} - \alpha_T \frac{n^3}{4} \frac{1+v}{1-v} (p_{11} + p_{12}) \quad (3)$$

where α_T is the thermal expansion, v is Poisson's ratio and p_{ii} is the element of the photoelastic tensor.

As described by Formulas (2) and (3), the optical and thermo-optical characteristics of several fluoride crystals, including a lower thermo-optical coefficient dn/dT , a smaller refractive index n and lower absorption loss, are favorable for reducing the thermal lensing effect. Starobor et al. reported a comparison of the thermal lensing effect of CeF₃, KTF and NTF crystals with that of a TGG crystal at the $\sim 1 \mu\text{m}$ spectral region [7]. As shown in Table 2, the required length of Faraday rotators of these crystals only slightly varies from 10.6 mm to 12.9 mm. The factor $\alpha P/\kappa$ of CeF₃, KTF and NTF crystals are negative due to the negative thermo-optical coefficients dn/dT of fluoride crystals. Considering the influence of the sample length, the magnitude of the factor $\alpha LP/\kappa$ of TGG is about $6.04 \times 10^{-8} \text{ W}^{-1}\cdot\text{m}$, about 6, 21 and 3 times larger than CeF₃, KTF and NTF, respectively. Thus, the thermal lensing effect of these fluoride magneto-optical crystals is much weaker than TGG, indicating they are promising Faraday rotators for high-power laser systems over kilowatt level.

Table 2. The comparison of thermal lensing effect between TGG and fluoride magneto-optical crystals [7].

	TGG	CeF ₃	KTF	NTF
Length of sample when $\theta = 45^\circ, B = 2T$ (mm)	10.6	10.8	11.2	12.9
$\frac{\alpha}{\kappa} P$ (10^{-8} W^{-1})	57	-8.9 ± 1.1	-2.5 ± 0.3	-14 ± 1.7
$\frac{\alpha L}{\kappa} P$ ($10^{-8} \text{ W}^{-1}\cdot\text{m}$)	6.04	-0.96 ± 0.12	-0.28 ± 0.02	-1.81 ± 0.22

Thermally induced depolarization is another kind of common thermal effect for magneto-optical crystals. The definition of depolarization γ can be expressed as [6]:

$$\gamma = \frac{P_d}{P_0} \quad (4)$$

where P_d is the depolarized light component after propagating the magneto-optical crystal. As the polarization of the reflected light beam is not completed perpendicular to the input polarizer of FI devices, the overall extinction value of IF devices will be decreased due to thermally induced depolarization.

The origin of thermally induced depolarization is the thermally induced birefringence due to inhomogeneous absorption or anisotropic thermal expansion, both increasing with the intensity of the propagated light beam. Therefore, the extinction value of IF devices will decrease when a more powerful light beam propagates. As reported in Reference [24], the CeF₃-based FI devices could still remain an isolation degree over 30 dB when the propagated laser power increases above 800 W, obviously higher than that of TGG-based devices (600 W).

4.2. The Performances of FI Devices based on Uniaxial Crystals

Traditional FI devices usually employ cubic crystals as Faraday isolators in order to avoid the effect of natural birefringence. The rotation angle of the major axis of the polarization ellipse has an oscillatory character that depends on the wavelength [55]. This characteristic, though often used to measure the Faraday rotation of a uniaxial or biaxial crystal, is of course unfavorable to achieving a high isolation degree in FI devices. Thus, the Faraday rotators of optical anisotropic magneto-optical materials must be fabricated along the optical axis.

Nevertheless, orientation deviations of uniaxial magneto-optical crystals are still common due to machining tolerance or crystals' inhomogeneity, which could result in a reduction in the isolation degree. The dependence of depolarization due to optical anisotropy is estimated in Ref. [24]. When the deviation between the laser propagation direction and the optical axis is small, the depolarization γ of a uniaxial crystal can be calculated by formula [24]:

$$\gamma = \sin^2 2\Psi \sin^2 \left(\frac{\pi L}{\lambda} \Delta n \rho^2 \right) \quad (5)$$

where Ψ is the polar angle counted from the direction of polarization, L is the length of the crystal and ρ is the deviation of laser propagation off the optical axis. For the uniaxial crystal CeF_3 , it is claimed that an isolation degree of over 30 dB can still be maintained in CeF_3 FI devices if the interval of the deviation of propagation orientation from the optical axis is smaller than 22 mrad or 1.26° , which is easy to achieve in practical usage [24]. As the crystallographic c axis cut samples are generally easy to fabricate, the applications of uniaxial magneto-optical crystals such as CeF_3 , PrF_3 and TLF for high-power IF devices are feasible.

5. Conclusions

The characteristics and developments of several fluoride magneto-optical crystals, including optically isotropic KTF and EuF_3 , uniaxial CeF_3 , PrF_3 and TLF, as well as biaxial TbF_3 , are introduced. The terbium-containing magneto-optical crystals, including KTF, TLF and TbF_3 , show comparable Verdet constants with TGG and similar transmittance spectral ranges. When propagated by a laser of 400 W, the thermal lensing effect and thermally induced depolarization effect of KTF-based FI device are obviously weaker than that of TGG-based one, indicating its advantages for application in high-power systems in the visible-to-NIR spectral region. CeF_3 crystals exhibit high transmittance continuously from 300 nm to 2.1 μm , thus could be used for FI devices from UV to mid-IR spectral range. Moreover, CeF_3 -based FI devices maintain high isolation degrees over 30 dB with a propagated laser power up to 800 W. On the other hand, PrF_3 and EuF_2 crystals are favorable for IF devices in the UV and mid-IR range, respectively, taking advantage of their high transmittances and large Verdet constants in these spectral regions. As the laser peak power and average power of high-power laser systems keep reaching higher levels and the wavelengths of solid-state lasers continue expanding to the UV and mid-IR spectral range, these fluoride magneto-optical crystals could find important applications in solid-state techniques.

Author Contributions: Writing—original draft preparation, Z.Z. (Zhonghan Zhang); writing—review and editing, A.W.; crystal growth and spectroscopic measurement of CeF_3 and PrF_3 , Z.Z. (Zhonghan Zhang), Z.W. and Z.Z. (Zhen Zhang); funding acquisition, L.S., A.W. and Z.Z. (Zhonghan Zhang); supervision, Y.L. and J.L. All authors have read and agreed to the published version of the manuscript.

Funding: This research was funded by the National Key Research and Development Program of China, grant number 2021YFB360150; the National Natural Science Foundation of China, grant number 52272014, and 62005302; the CAS Project for Young Scientists in Basic Research, grant number YSBR-024; Shanghai Science and Technology Commission, grant number 21520711300, and

22ZR1472000; Opening Project of the Ninth Research Institute of China Electronics Technology Group Corporation, grant number 2022SK-013; Science Foundation for Youth Scholar of State Key Laboratory of High Performance Ceramics and Superfine Microstructures, grant number SKL201904.

Institutional Review Board Statement: Not applicable.

Informed Consent Statement: Not applicable.

Data Availability Statement: Not applicable.

Conflicts of Interest: The authors declare no conflict of interest.

References

1. Dötsch, H.; Bahlmann, N.; Zhuromskyy, O.; Hammer, M.; Wilkens, L.; Gerhardt, R.; Hertel, P.; Popkov, A.F. Applications of magneto-optical waveguides in integrated optics: Review. *J. Opt. Soc. Am. B* **2005**, *22*, 240–253. [\[CrossRef\]](#)
2. Stadler, B.J.H.; Mizumoto, T. Integrated Magneto-Optical Materials and Isolators: A Review. *IEEE Photonics J.* **2014**, *6*, 1–15. [\[CrossRef\]](#)
3. Snetkov, I.L.; Viotovich, A.V.; Palashov, O.V.; Khazanov, E.A. Review of Faraday Isolators for Kilowatt Average Power Lasers. *IEEE J. Quantum Electron.* **2014**, *50*, 434–443. [\[CrossRef\]](#)
4. Vojna, D.; Slezák, O.; Lucianetti, A.; Mocek, T. Verdet Constant of Magneto-Active Materials Developed for High-Power Faraday Devices. *Appl. Sci.* **2019**, *9*, 3160. [\[CrossRef\]](#)
5. Schulz, P.A. Wavelength independent Faraday isolator. *Appl. Opt.* **1989**, *28*, 4458–4464. [\[CrossRef\]](#)
6. Mironov, E.A.; Starobor, A.V.; Snetkov, I.L.; Palashov, O.V.; Furuse, H.; Tokita, S.; Yasuhara, R. Thermo-optical and magneto-optical characteristics of CeF₃ crystal. *Opt. Mater.* **2017**, *69*, 196–201. [\[CrossRef\]](#)
7. Starobor, A.; Mironov, E.A.; Palashov, O.V. Thermal lens in magneto-active fluoride crystals. *Opt. Mater.* **2019**, *98*, 109469. [\[CrossRef\]](#)
8. Vojna, D.; Slezák, O.; Yasuhara, R.; Furuse, H.; Lucianetti, A.; Mocek, T. Faraday Rotation of Dy₂O₃, CeF₃ and Y₃Fe₅O₁₂ at the Mid-Infrared Wavelengths. *Materials* **2020**, *13*, 5324. [\[CrossRef\]](#)
9. Carothers, K.J.; Norwood, R.A.; Pyun, J. High Verdet Constant Materials for Magneto-Optical Faraday Rotation: A Review. *Chem. Mater.* **2022**, *34*, 2531–2544. [\[CrossRef\]](#)
10. Mironov, E.A.; Zhelezov, D.S.; Starobor, A.V.; Voitovich, A.V.; Palashov, O.V.; Bulkanov, A.M.; Demidenko, A.G. Large-aperture Faraday isolator based on a terbium gallium garnet crystal. *Opt. Lett.* **2015**, *40*, 2794–2797. [\[CrossRef\]](#) [\[PubMed\]](#)
11. Molina, P.; Vasylyev, V.; Shimamura, K. CeF₃ and PrF₃ as UV-Visible Faraday rotators. *Opt. Express* **2011**, *19*, 11786–11791. [\[CrossRef\]](#)
12. Srinivasan, K.; Stadler, B.J.H. Magneto-optical materials and designs for integrated TE- and TM-mode planar waveguide isolators: A review. *Opt. Mater. Express* **2018**, *8*, 3307–3318. [\[CrossRef\]](#)
13. Krinchik, G.S.; Chetkin, M.V. Transparent Ferromagnets. *Sov. Phys. Uspekhi* **1969**, *12*, 307–319. [\[CrossRef\]](#)
14. Komatsu, H. Mechanism of crystal growth of yttrium-ion garnet and magnetoplumbite synthesized by flux method. *Miner. J.* **1964**, *4*, 203–211. [\[CrossRef\]](#)
15. Kimura, S.; Shindo, I. Single crystal growth of YIG by the floating zone method. *J. Cryst. Growth* **1977**, *41*, 192–198. [\[CrossRef\]](#)
16. Hibiya, T. Liquid phase epitaxial growth of thick garnet films—“Perfectness” of crystal quality. *J. Magn. Soc. Jpn.* **1987**, *11*, 167–172. [\[CrossRef\]](#)
17. Dai, J.; Li, J. Promising magneto-optical ceramics for high power Faraday isolators. *Scr. Mater.* **2018**, *155*, 78–84. [\[CrossRef\]](#)
18. Jalali, A.A.; Rogers, E.; Stevens, K. Characterization and extinction measurement of potassium terbium fluoride single crystal for high laser power applications. *Opt. Lett.* **2017**, *42*, 899–902. [\[CrossRef\]](#)
19. Starobor, A.V.; Mironov, E.A.; Palashov, O.V.; Savelyev, A.G.; Karimov, D.N. Dispersion of optical and magneto-optical properties in a biaxial TbF₃ crystal. *Laser Phys. Lett.* **2021**, *18*, 115801. [\[CrossRef\]](#)
20. Vasylyev, V.; Villora, E.G.; Nakamura, M.; Sugahara, Y.; Shimamura, K. UV-visible Faraday rotators based on rare-earth fluoride single crystals: LiREF₄ (RE = Tb, Dy, Ho, Er and Yb), PrF₃ and CeF₃. *Opt. Express* **2012**, *20*, 14460–14470. [\[CrossRef\]](#)
21. Snetkov, I.L. Features of Thermally Induced Depolarization in Magneto-Active Media With Negative Optical Anisotropy Parameter. *IEEE J. Quantum Electron.* **2018**, *54*, 7000108. [\[CrossRef\]](#)
22. Mironov, E.A.; Palashov, O.V.; Karimov, D.N. EuF₂-based crystals as media for high-power mid-infrared Faraday isolators. *Scr. Mater.* **2019**, *162*, 54–57. [\[CrossRef\]](#)
23. Starobor, A.; Mironov, E.; Snetkov, I.; Palashov, O.; Furuse, H.; Tokita, S.; Yasuhara, R. Cryogenically cooled CeF₃ crystal as media for high-power magneto-optical devices. *Opt. Lett.* **2017**, *42*, 1864–1866. [\[CrossRef\]](#) [\[PubMed\]](#)
24. Starobor, A.; Mironov, E.; Palashov, O. High-power Faraday isolator on a uniaxial CeF₃ crystal. *Opt. Lett.* **2019**, *44*, 1297–1299. [\[CrossRef\]](#)
25. Berger, S.B.; Rubinstein, C.B.; Kurkjian, C.R.; Treptaw, A.W. Faraday Rotation of Rare-Earth (III) Phosphate Glasses. *Phys. Rev.* **1964**, *133*, A723–A727. [\[CrossRef\]](#)
26. Stevens, K.T.; Schlichting, W.; Foundos, G.; Payne, A.; Rogers, E. Promising Materials for High Power Laser Isolators. *Laser Tech. J.* **2016**, *3*, 18–21. [\[CrossRef\]](#)

27. Griffin, J.A.; Folkens, J.; Weber, M.J.; Morgret, R.; Litster, J.D.; Gabbe, D.; Linz, A. Magnetic, optical, and magneto-optical behavior of LiTbF_4 and $\text{KTb}_3\text{F}_{10}$ crystals. *J. Appl. Phys.* **1978**, *49*, 2209–2211. [[CrossRef](#)]
28. Weber, M.J.; Morgret, R.; Leung, S.Y.; Griffin, J.A.; Gabbe, D.; Linz, A. Magneto-optical properties of $\text{KTb}_3\text{F}_{10}$ and LiTbF_4 crystals. *J. Appl. Phys.* **1978**, *49*, 3464–3469. [[CrossRef](#)]
29. Abbasalizadeh, A.; Sridar, S.; Chen, Z.; Sluiter, M.; Yang, Y.; Sietsma, J.; Seetharaman, S.; Hari Kumar, K.C. Experimental investigation and thermodynamic modelling of $\text{LiF-NdF}_3\text{-DyF}_3$ system. *J. Alloy. Compd.* **2018**, *753*, 388–394. [[CrossRef](#)]
30. Zelmon, D.E.; Erdman, E.C.; Stevens, K.T.; Foundos, G.; Kim, J.R.; Brady, A. Optical properties of lithium terbium fluoride and implications for performance in high power lasers. *Appl. Opt.* **2016**, *55*, 834–837. [[CrossRef](#)]
31. Kukharchyk, N.; Sholokhov, D.; Morozov, O.; Korableva, S.L.; Kalachev, A.A.; Bushev, P.A. Optical coherence of $^{166}\text{Er}:\text{LiYF}_4$ crystal below 1 K. *New J. Phys.* **2018**, *20*, 023044. [[CrossRef](#)]
32. Karimov, D.N.; Buchinskaya, I.I. Growth of KR_3F_{10} ($\text{R} = \text{Tb-Er}$) Crystals by the Vertical Directional Crystallization Technique. I: Optimization of the Melt Composition for the Growth of $\text{KTb}_3\text{F}_{10}$ and Correction of the Phase Diagram of the KF-TbF_3 System. *Crystallogr. Rep.* **2021**, *66*, 535–540. [[CrossRef](#)]
33. Karimov, D.N.; Buchinskaya, I.I.; Arkharova, N.A.; Ivanova, A.G.; Savelyev, A.G.; Sorokin, N.I.; Popov, P.A. Growth Peculiarities and Properties of KR_3F_{10} ($\text{R} = \text{Y, Tb}$) Single Crystals. *Crystals* **2021**, *11*, 285. [[CrossRef](#)]
34. Furuse, H.; Yasuhara, R.; Hiraga, K. Thermo-optic effects of ceramic TGG in the 300–500 K temperature range. *Opt. Mater. Express* **2015**, *5*, 1266. [[CrossRef](#)]
35. Yasuhara, R.; Tokita, S.; Kawanaka, J.; Kawashima, T.; Kan, H.; Yagi, H.; Nozawa, H.; Yanagitani, T.; Fujimoto, Y.; Yoshida, H.; et al. Measurement of magneto-optical property and thermal conductivity on TGG ceramic for Faraday material of high-peak and high average power laser. *Rev. Laser Eng.* **2007**, *35*, 806–810. [[CrossRef](#)]
36. Valiev, U.V.; Karimov, D.N.; Burdick, G.W.; Rakhimov, R.; Pelenovich, V.O.; Fu, D. Growth and magneto-optical properties of anisotropic TbF_3 single crystals. *J. Appl. Phys.* **2017**, *121*, 243105. [[CrossRef](#)]
37. Karimov, D.N.; Lisovenko, D.S.; Ivanova, A.G.; Grebenev, V.V.; Popov, P.A.; Sizova, N.L. Bridgman Growth and Physical Properties Anisotropy of CeF_3 Single Crystals. *Crystals* **2021**, *11*, 793. [[CrossRef](#)]
38. Laiho, R.L.; Lakkisto, M. Investigation of the refractive indices of LaF_3 , CeF_3 , PrF_3 , and NdF_3 . *Philos. Mag. B* **1983**, *48*, 203–207. [[CrossRef](#)]
39. Popov, P.A.; Moiseev, N.V.; Karimov, D.N.; Sorokin, N.I.; Sulyanova, E.A.; Sobolev, B.P. Thermophysical Characteristics of $\text{EuF}_{2.136}$ Crystal. *Crystallogr. Rep.* **2015**, *60*, 740–743. [[CrossRef](#)]
40. Shannon, R.D.; Shannon, R.C.; Medenbach, O.; Fischer, R.X. Refractive Index and Dispersion of Fluorides and Oxides. *J. Phys. Chem. Ref. Data* **2002**, *31*, 931–970. [[CrossRef](#)]
41. Karimov, D.N.; Sobolev, B.P.; Ivanov, I.A.; Kanorsky, S.I.; Masalov, A.V. Growth and Magneto Optical Properties of $\text{Na}_{0.37}\text{Tb}_{0.63}\text{F}_{2.26}$ Cubic Single Crystal. *Crystallogr. Rep.* **2014**, *59*, 718–723. [[CrossRef](#)]
42. Mironov, E.A.; Palashov, O.V.; Voitovich, A.V.; Kaminov, D.N.; Ivanov, I.A. Investigation of thermo-optical characteristics of magneto-active crystal $\text{Na}_{0.37}\text{Tb}_{0.63}\text{F}_{2.26}$. *Opt. Lett.* **2015**, *40*, 4919–4922. [[CrossRef](#)]
43. Mironov, E.A.; Palashov, O.V.; Naumov, A.K.; Aglyamov, R.D.; Semashko, V.V. Faraday isolator based on NTF crystal in critical orientation. *Appl. Phys. Lett.* **2021**, *119*, 073502. [[CrossRef](#)]
44. Allain, J.L.; Couchaud, M.; Ferrand, B.; Grange, Y.; Utts, B.; Wyon, C. Crystal Growth and Scintillation Properties of CeF_3 . *Mat. Res. Soc. Symp. Proc.* **1994**, *348*, 105–110. [[CrossRef](#)]
45. Belli, P.; Bernabei, R.; Cerulli, R.; Dai, C.J.; Danevich, F.A.; Incicchitti, A.; Kobychov, V.V.; Ponkratenko, O.A.; Prospero, D.; Tretyak, V.I.; et al. Performances of a CeF_3 crystal scintillator and its application to the search for rare processes. *Nucl. Instrum. Methods Phys. Res. A* **2003**, *498*, 352–361. [[CrossRef](#)]
46. Dissertori, G.; Lecomte, P.; Luckey, D.; Nessi-Tedaldi, F.; Pauss, F.; Otto, T.S.; Roesler, S.; Urscheler, C. A study of high-energy proton induced damage in cerium fluoride in comparison with measurements in lead tungstate calorimeter crystals. *Nucl. Instrum. Methods Phys. Res. Sect. A Accel. Spectrometers Detect. Assoc. Equip.* **2010**, *622*, 41–48. [[CrossRef](#)]
47. Nakagawa, K.; Asahi, T. Determination of the Faraday rotation perpendicular to the optical axis in uniaxial CeF_3 crystal by using the Generalized-High Accuracy Universal Polarimeter. *Sci. Rep.* **2019**, *9*, 18453. [[CrossRef](#)]
48. Vojna, D.; Yasuhara, R.; Slezák, O.; Mužík, J.; Lucianetti, A.; Mocek, T. Verdet constant dispersion of CeF_3 in the visible and near-infrared spectral range. *Opt. Eng.* **2017**, *56*, 067105. [[CrossRef](#)]
49. Li, H.; Wang, J.; Chen, J.; Dai, Y.; Su, L.; Li, X.; Kalashnikova, M.; Wu, A. Bridgman growth and magneto-optical properties of CeF_3 crystal as Faraday Rotator. *Opt. Mater.* **2020**, *100*, 109675. [[CrossRef](#)]
50. Yan, X.; Liu, Q.; Chen, H.; Fu, X.; Gong, M.; Wang, D. 35.1 W all-solid-state 355 nm ultraviolet laser. *Laser Phys. Lett.* **2020**, *7*, 563. [[CrossRef](#)]
51. Villora, E.G.; Shimamura, K.; Plaza, G.R. Ultraviolet-visible optical isolators based on CeF_3 Faraday rotator. *J. Appl. Phys.* **2015**, *117*, 233101. [[CrossRef](#)]
52. Danson, C.N.; Haefner, C.; Bromage, J.; Butcher, T.; Chanteloup, J.-C.F.; Chowdhury, E.A.; Galvanauskas, A.; Gizzi, L.A.; Hein, J.; Hillier, D.I.; et al. Petawatt and exawatt class lasers worldwide. *High Power Laser Sci. Eng.* **2017**, *7*, e54. [[CrossRef](#)]
53. Federov, P.P.; Sobolev, B.P. Morphotropic transitions in the rare-earth trifluoride series. *Crystallogr. Rep.* **1995**, *40*, 315–321.

54. Jiang, G.; Zhang, Z.; Li, H.; Shen, H.; Wu, A.; Li, J.; Wang, J.; Su, L.; Xu, J. TGT growth and magneto-optical properties of PrF₃ crystal. *Phys. B Phys. Condens. Matter* **2021**, *614*, 413031. [[CrossRef](#)]
55. Valiev, U.V.; Uzokov, A.A.; Rakhimov, S.A.; Gruber, J.B.; Nash, K.L.; Sardar, D.K.; Burdick, G.W. Faraday effect and magnetic susceptibility analyses in TbAlO₃. *J. Appl. Phys.* **2008**, *104*, 073903. [[CrossRef](#)]

Disclaimer/Publisher's Note: The statements, opinions and data contained in all publications are solely those of the individual author(s) and contributor(s) and not of MDPI and/or the editor(s). MDPI and/or the editor(s) disclaim responsibility for any injury to people or property resulting from any ideas, methods, instructions or products referred to in the content.